JOURNAL OF SOLID STATE CHEMISTRY 104, 359–367 (1993)

Iron-Substituted Nickel Oxyhydroxides and Hydroxides Obtained by Chimie Douce

L. DEMOURGUES-GUERLOU, J. J. BRACONNIER, AND C. DELMAS*

Laboratoire de Chimie du Solide du CNRS and Ecole Nationale Supérieure de Chimie et Physique de Bordeaux, Université de Bordeaux I, 351, cours de la Libération, 33405 Talence Cedex, France

Received March 18, 1992; in revised form October 21, 1992; accepted October 26, 1992

New iron-substituted nickel hydroxides have been prepared by chimie douce reactions from the $NaNi_{1-x}Fe_xO_2$ precursor phases. Oxidizing hydrolysis of these materials leads to γ-oxyhydroxides which are then easily reduced to hydroxides. A crystal chemical study of the three material classes has been performed. The precursor phases crystallize in the rhombohedral system for $x \geq 0.2$, while the lower iron concentrations lead to a monoclinic distortion due to the Jahn–Teller effect of Ni^{III} ions. This distortion is not observed in the case of the γ phases. For $x \geq 0.2$, the hydroxides also crystallize in the rhombohedral system, whereas for smaller iron concentrations, interstratified-type structures similar to those commonly found among the layered double hydroxide minerals family are obtained. Chemical analysis and magnetic property study have shown the presence of $(1 - x)Ni^{2+}$ and xFe^{3+} ions within the slab. Anions (mainly CO_3^{2-} ions) are inserted into the intersheet space in order to compensate the excess positive charge due to Fe^{3+} ions.

Introduction

Several nickel hydroxide varieties are involved as positive electrode materials in the electrochemical cycling that occurs in Ni/Cd and Ni/H_2 batteries, as shown by the following well-known Bode diagram (*1*):

	Electrochemical	
β(II)-$Ni(OH)_2$	⇄	β(III)-NiOOH
↑	cycling	↓ Cell overcharge
α-$Ni(OH)_2,zH_2O$	⇄	γ-"NiOOH"

The structure of the above-mentioned phases can be described as a packing of NiO_2 slabs built up of edge-sharing octahedra. In commercial batteries, the classical cycling takes place between the β(II)- and β(III)-phases but long term overcharge or floating leads to the formation of the hydrated γ variety by intercalation of water molecules and K^+ ions in the interslab space. Such a process, if repeated during cycling, causes mechanical strains in the material and therefore irreversible damage to the electrode. The stabilization of the cycling between the hydrated α and γ varieties, as a means of inhibiting this problem, seems very promising.

Previous works performed in our lab have shown that the partial substitution of cobalt for nickel leads, using chimie douce tech-

* To whom correspondence should be addressed.

0022-4596/93 $5.00

niques, to well-crystallized hydrated α^* and γ nickel hydroxides (*2*). As previously reported, the α^* notation refers to well-crystallized materials while α corresponds to turbostratic materials obtained by direct precipitation (*2*). For cobalt/(nickel + cobalt) ratios larger than 20%, the α^* phase is stable in KOH electrolyte at room temperature and the α^*/γ system is stabilized during the electrode cycling in Ni/Cd batteries (*3*). In the reduced α^*-phase, the cobalt ions stay in the trivalent state while the nickel ones are divalent. In order to compensate the excess of positive charge due to the Co^{III} ions within the slab, anions are inserted into the intersheet space (*4*). The composition and the structure of these materials are strongly related to the hydrotalcite ones (*5*). In the oxidized γ-phases containing up to 40% cobalt in substitution for nickel, the nickel ions are in the trivalent and tetravalent states whereas the cobalt ones stay only in the trivalent state (*6*). Consequently, the cobalt ions do not directly take part in the α^*/γ cycling. Hence, a similar study of the homologous iron-substituted materials has been undertaken.

Mendiboure and Schöllhorn have recently reported the study of the hydrotalcite-type compounds $Ni_{1-x}Fe_x(OH)_2(CO_3)_{x/2}(H_2O)_z$ (*7*). For $x = 0.25$, this formula is identical to that of the mineral reevesite (*8, 9*). These authors have focused their interest on the anion exchange reactions, around the $x = 0.25$ composition, in materials prepared by direct precipitation which are consequently poorly crystallized.

In order to obtain a large particle size making the X-ray diffraction characterization easier, we have used chimie douce techniques. Moreover, all the Fe/Ni possible compositions have been considered. The various materials involved in the synthesis are presented in this paper from the crystal chemistry viewpoint. Besides, the investigation of the oxidation state of the 3*d* cations in the iron-substituted γ-phases has proved unambiguously the presence of tetravalent iron ions (*10*). These results will be described in more detail in a forthcoming paper. The present paper deals more particularly with the characterization of the iron-substituted α^*-phases.

Material Preparation

The preparation procedure consists of exchange, oxidation, and reduction reactions involving successively three material classes:

—the $NaNi_{1-x}Fe_xO_2$ precursor phases
—the iron-substituted γ-oxyhydroxides
—the iron-substituted α^*-hydroxides.

Preparation of Iron-Substituted Sodium Nickelates

These materials have been prepared by direct reaction from the oxides according to the reaction

$$(1/2)Na_2O + (1 - x)NiO + (x/2)Fe_2O_3 + (1/4 - x/4)O_2 \rightarrow NaNi_{1-x}Fe_xO_2.$$

The oxide mixture is heated at 800°C for 15 hr in an alumina boat under an oxygen stream.

Hydrolysis Reaction: Preparation of γ-Oxyhydroxides

A quantity of 1 g of $NaNi_{1-x}Fe_xO_2$ (sodium nickelate) is introduced into 100 ml of oxidizing hydrolysis solution (4 *M* KOH, 0.8 *M* NaClO). The mixture is stirred for 15 hr. The resulting material is then filtered and dried at 40°C. Due to the highly oxidizing character of the obtained material, any washing with water is prohibited. Indeed, the material tends to be spontaneously reduced by water.

Reduction Reaction: Preparation of α^*-Hydroxide

A quantity of 50 ml of a 0.5 *M* H_2O_2 solution is gradually dropped into a solution containing 1 g of γ-oxyhydroxide in suspension in 100 ml of water. After stirring for 15 hr,

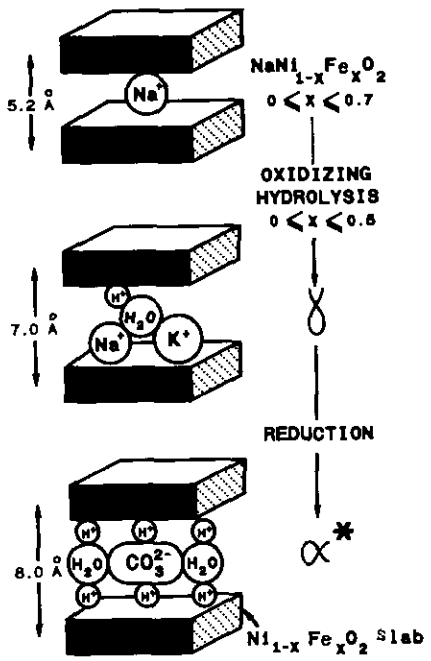

FIG. 1. Formation of the α^*-phase by chimie douce reactions.

the obtained material is filtered, washed with distilled water then with acetone and dried at 40°C.

Results and Discussion

Figure 1 gives an overview of the composition and schematic structure modifications involved during the chimie douce reactions from the $NaNi_{1-x}Fe_xO_2$ precursor phase.

Crystal Chemistry

The Iron-Substituted Sodium Nickelates

The crystal chemistry of these materials is quite similar to that observed in the case of the homologous cobalt-substituted phases (*2*). A pure black phase with $NaNi_{1-x}Fe_xO_2$ formulation has been prepared for $0 \leq x \leq 0.70$. For higher iron concentrations, a mixture of the limit composition and α-$NaFeO_2$ is obtained, even after several thermal treatments. Both materials are isotypic and moreover exhibit close hexagonal unit cell parameters:

$a = 3.020$ Å and $c = 16.08$ Å for α-$NaFeO_2$

$a = 3.000$ Å and $c = 16.00$ Å for

the $NaNi_{0.3}Fe_{0.7}O_2$ limit composition.

Similar behavior has been observed with the $NaNi_{1-x}Co_xO_2$ system, but in this case the upper limit of the solid solution is $NaNi_{0.5}Co_{0.5}O_2$ (*6*).

A change in symmetry occurs around the $NaNi_{0.8}Fe_{0.2}O_2$ composition. For $x \geq 0.2$, the materials crystallize in the rhombohedral system like α-$NaFeO_2$ (S.G.: $R\bar{3}m$), while for $x < 0.2$, a monoclinic distortion similar to that of the unsubstituted $NaNiO_2$ phase is observed as a result of the strong Jahn–Teller effect of the low-spin Ni^{III} (LS) ions, which is quite general in layer oxides containing more than 80% Jahn–Teller ions (*11*). In these materials with layered structure, the Na^+ ions occupy an octahedral environment between the $(Ni,Fe)O_2$ slabs. The O'3 type packing of oxygen layers characterizes the distorted phases whereas the O3 type is observed for the undistorted ones (*12*).

This change in symmetry is particularly well illustrated by the variation of the metal–metal intrasheet distance reported in Fig. 2a. The cooperative distortion is emphasized for $x < 0.2$ by the presence of two different *M–M* intrasheet distances directly related to the $a_{mon.}$ and $b_{mon.}$ parameters. For $x \geq 0.2$, the increase with x in the metal–metal intrasheet distance, which is equal to the hexagonal a-parameter, results from the size difference between high-spin Fe^{3+} (HS) and Ni^{III} (LS) ions ($r_{Fe^{3+}(HS)} = 0.64$ Å, $r_{Ni^{III}(LS)} = 0.56$ Å) (*13*). In the homologous cobalt-substituted phases, the smaller size of the Co^{III} (LS) ions in comparison with that of the Ni^{III} ones implies a decrease in the *M–M* intrasheet distance.

The variation with x of the interslab dis-

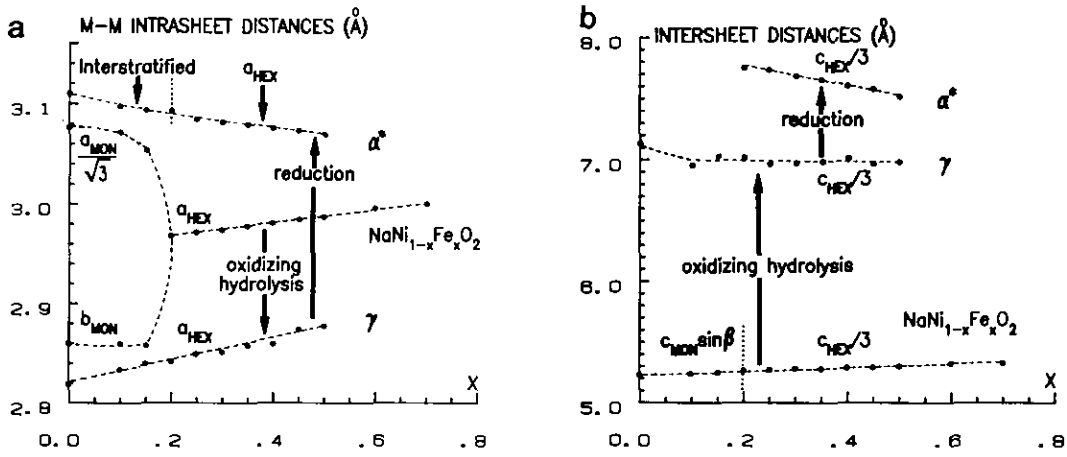

FIG. 2. Variation of metal–metal intrasheet distances (a) and intersheet distances (b) vs iron concentration during the chimie douce reactions.

tance, equal either to $c_{mon.} \sin \beta$ ($x < 0.2$) or to $c_{hex.}/3$ ($0.2 \leq x \leq 0.7$), is reported in Fig. 2b. The slight increase observed may also result from the size difference between the nickel and iron ions.

The Iron-Substituted γ-Oxyhydroxides

These materials have been obtained by oxidizing hydrolysis from the $NaNi_{1-x}Fe_xO_2$ phases for $0 \leq x \leq 0.5$. For larger iron concentrations, the reaction leads to a mixture of several phases as the presence of a large amount of iron makes difficult the oxidation of the material. As previously noticed in the case of the cobalt-substituted γ-phases (*2*), the iron-substituted materials crystallize in the rhombohedral system (S.G.: *R*3*m*) with a *P*3 type oxygen packing. The monoclinic distortion previously described for the $NaNi_{1-x}Fe_xO_2$ phases for $x < 0.2$ is no more observed whatever the iron concentration.

Figure 2 gives evidence of the strong lattice parameter modifications that occur during the oxidizing hydrolysis reaction. The strong increase in the interslab distance is due to the intercalation between the slabs (as schematized in Fig. 1) of K^+ ions solvated by water molecules. Moreover, the oxidation of the 3*d* cations induces a strong decrease in the *a*-parameter (metal–metal intrasheet distance). Besides, in the iron-substituted γ-phase, the metal–metal distance tends to increase with increasing *x*, which results from the size difference between nickel and iron ions: whatever the oxidation state of both ions (+3 or +4), the iron ions are larger than the nickel ones (*13*). Different behavior has been noticed in the cobalt-substituted γ-phases (*6*): no significant variation of the *a*-parameter with *x* was detected, whereas the values of ionic radius should imply a decrease. This effect has to be correlated with the fact that the *a*-parameter value of the unsubstituted γ phase (2.82 Å) is close to the minimal distance between two O^{2-} ions ($r_{O^{2-}} = 1.40$ Å (*13*)). As a consequence, the lattice is virtually close-packed in the plane, which prevents any contraction upon substitution of cobalt for nickel.

The γ-phases exhibit the general formula

$$\underbrace{H_yNa_uK_w(H_2O)_z}_{\text{Interslab space}} \quad \underbrace{Ni_{1-x}Fe_xO_2}_{\text{Slab}}$$

but the material instability makes difficult the exact formula determination. The exact

bonding nature of hydrogen inserted between NiO_2 slabs is not known at this time. Several hypotheses can be envisaged:

—bonding to an oxygen atom of a NiO_2 slab (formation of OH group),

—bonding to an interlamellar water molecule (formation of H_3O^+ ions),

—insertion in oxygen octahedra in the interslab space as reported for hydrogen insertion in γ-MnO_2 (*14*).

A study of the dynamics of hydrogen by inelastic neutron scattering is scheduled in order to precise this point. In Fig. 1 as well as in the above proposed formula, we have assumed the presence of H^+ species for simplification. Moreover these materials do not have a strictly defined formula as they exhibit a wide composition range. The average oxidation state of the metal cations lies in the 3.35–3.65 range. The results concerning the investigation by magnetic measurement and Mössbauer spectroscopy of the oxidation state of both the nickel and iron ions will be published in a forthcoming paper (*15*).

The Iron-Substituted Hydroxides

Reduction of the iron-substituted γ-phases has led to the corresponding hydroxides for $0 \leq x \leq 0.50$. Their color varies from pale brown to dark brown with increasing iron concentration.

• For $x \geq 0.2$, α^*-type phases have been obtained. These materials are isostructural with the unsubstituted α^*-$Ni(OH)_2,zH_2O$ hydroxide previously studied in our laboratory (*16*).

Comparison of the X-ray diffraction pattern we obtained for $x = 0.25$ with that corresponding to the $Ni_{0.75}Fe_{0.25}(OH)_2(CO_3)_{0.125}(H_2O)_z$ recently obtained by precipitation by Mendiboure and Schöllhorn (*7*) shows a strong similarity between the two materials. Nevertheless, as expected, the material that we prepared by chimie douce techniques exhibits a better crystallization state than the precipitated one. Besides, our material is very similar to the mineral reevesite (*8, 9*), in spite of minor differences concerning the indexation of the X-ray diffraction spectra: the iron-substituted α^* phases we obtained crystallize in the rhombohedral system with a *P*3 type-packing of oxygen layers while the reevesite exhibits a double hexagonal unit cell (6 slabs per unit cell). This behavior may result from the existence of an order in the lattice due to the $x = 0.25$ value. X-ray diffraction data obtained from the α^* phase for $x = 0.3$ have been summarized in Table I.

TABLE I

X-RAY DIFFRACTION DATA FOR THE α^* ($x = 0.3$) PHASE

h k l	$d_{calc.}$	$d_{obs.}$	Intensity
0 0 3	7.69	7.63	100
0 0 6	3.84	3.83	25
0 1 2	2.598	2.601	16
1 0 4	2.421	2.417	1
0 1 5	2.309	2.307	5
0 1 8	1.958	1.961	2
1 0 10	1.745	1.745	1
0 1 11	1.649	1.653	1
1 1 0	1.540	1.540	1
1 1 3	1.510	1.510	1

Note. The indexation has been performed on a hexagonal unit cell with $a = 3.080$ Å, $c = 23.07$ Å

The variations with x of the metal–metal intrasheet and intersheet distances, both related to the parameters of the hexagonal cell, are also presented in Fig. 2. These variations result from the oxidation state of the cations within the slab, in other words, from the presence of Fe^{3+} ions substituted for Ni^{2+} ions, as shown by the results reported in the following section. The metal–metal intrasheet distance decreases with x, as a result of the ionic radius difference between Ni^{2+} ($r_i = 0.70$ Å) and Fe^{3+} (HS) ($r_i = 0.64$ Å) ions (*13*). Moreover, the increase in the electrostatic charge of the slab with the iron concentration, as improving the intersheet cohesivness, induces a decrease in the intersheet distance.

• For $x < 0.2$, the X-ray diffraction pat-

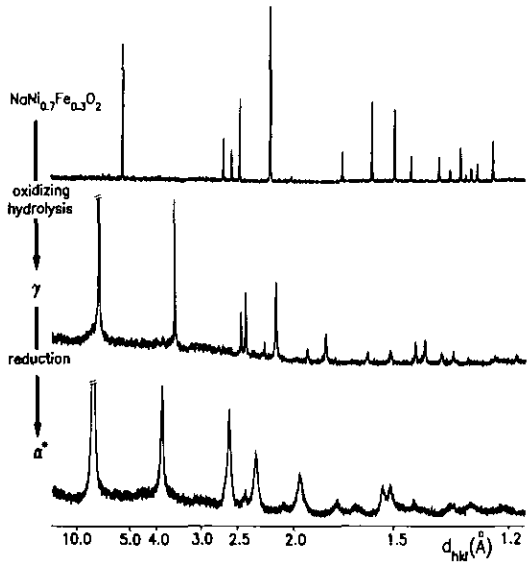

FIG. 3. X-ray diffraction spectra ($CoK\alpha_1$) of the $NaNi_{0.7}Fe_{0.3}O_2$, γ and α^* phases.

terns cannot be indexed, although exhibiting strong similarities with those obtained for $x \geq 0.2$. The discrepancy between the observed and calculated d_{hkl} ($l \neq 0$) values, the peculiar shape of the diffraction lines and the similarities with the homologous cobalt-substituted materials previously studied (*6*, *16*) are characteristic of the existence of an interstratified structure. Nevertheless, the metal–metal intrasheet distance can be determined as it remains equal to twice the interplanar distance homologous to the d_{110} one in well-ordered materials.

Figure 2 gives evidence of the modifications in the lattice parameters involved during reduction from the γ oxyhydroxides to the hydroxides: the metal–metal intrasheet and intersheet distances increase as a result of the changes in cationic oxidation state and in interlab space respectively (schematized in Fig. 1). Moreover, Fig. 3 makes it possible to compare the X-ray diffraction spectrum of the α^* ($x = 0.3$) phase with those of the $NaNi_{0.7}Fe_{0.3}O_2$ and γ parent phases. The chimie douce reactions and more particularly the reduction entail a material grinding which appears on the spectra through a line broadening.

Characterization of the Iron-Substituted Hydroxides

The determination of the 3*d* cation oxidation state in both the oxidized (γ) and reduced varieties (α) holds interest since the electrochemical activity is strongly related to it. In the α^* phases the iron ions are likely to be trivalent, similarly to the case of cobalt substitution (*2*). This hypothesis has been confirmed by chemical analysis and magnetic susceptibility measurements, as described hereafter. In the mineral reevesite, which exhibits the formula $H_2(H_2O)_{0.5}(CO_3)_{0.125}Fe_{0.25}Ni_{0.75}O_2$ (*8*, *9*), carbonate ions are inserted into the interslab space in order to compensate the excess of positive charge resulting from the presence of Fe^{3+} cations within the slab. This behavior, already observed in the cobalt-substituted nickel hydroxides (*2*), is also verified in the case of iron substitution. In both cases, the CO_3^{2-} anions originate directly from CO_2 of air. Indeed, the chemical analysis of the α^* materials leads as an example for $x = 0.30$ to the following formula:

$$\underbrace{H_{2.02}(H_2O)_{0.61}(CO_3)_{0.16}}_{\text{Interslab Space}} \qquad \underbrace{Ni_{0.70}Fe_{0.30}O_2}_{\text{Slab}}$$

Moreover, the presence of carbonate anions is confirmed by infrared spectroscopy (see further).

3d Cation Oxidation State

The average oxidation state of the metal cations in the slab has been determined by iodometry. For this purpose, the sample (powder) is dissolved into a mixture of HCl and KI. The iodine released during the cationic reduction to the divalent state is then rapidly titrated by 0.1 N–$Na_2S_2O_3$ in the presence of thiodene. The titration is performed in air. The amount of titrated iodine allows to easily deduce the average cationic

TABLE II

AVERAGE OXIDATION STATE OF THE TRANSITION IONS IN THE NICKEL HYDROXIDES VERSUS IRON CONCENTRATION (IN ION g/mole)

x	0.10	0.20	0.30	0.40	0.50
Oxidation state ± 0.05	2.16	2.27	2.40	2.47	2.55

oxidation state of the material. The results are summarized in Table II. The value of the uncertainty of the oxidation state reported in Table II results from the discrepancies between the experimental results. The exact reason of these quite large uncertainties is unknown.

Table II shows that the oxidation state of the transition ions in the iron-substituted hydroxides is close to $2 + x$, which suggests the presence of $(1 - x)Ni^{2+}$ and xFe^{3+} ions within the slabs.

This result is corroborated by the ^{57}Fe Mössbauer spectroscopy study of the α^* ($x = 0.3$) phase reported elsewhere (10) as well as by the magnetic susceptibility measurements performed for iron concentrations ranging from 0.1 to 0.5.

Magnetic susceptibility measurements have been carried out with a DSM8 susceptometer (MANICS) over the 4–300 K temperature range (average magnetic field of 18 kG). The sample was placed in a PTFE crucible. The thermal variation of the χ_M^{-1} reciprocal molar susceptibility is given in Fig. 4 as an example for the α^*-phases with $x = 0.2$ and $x = 0.5$. The curve shapes are characteristic of Curie–Weiss type laws with small values of the Curie temperature. Table III summarizes the experimental values of the Curie constants that have been deduced from the linear parts of the curves ($T > 60$ K) as well as the theoretical values calculated by assuming the presence of xFe^{3+} (HS) ions and $(1 - x)Ni^{2+}$ ions within the slab. The experimental values are close to the theoretical ones for iron concentrations up to 0.4. Nevertheless the difference between both values increases slightly with x and becomes significant for $x = 0.5$. An understanding of this effect has not been achieved at this time.

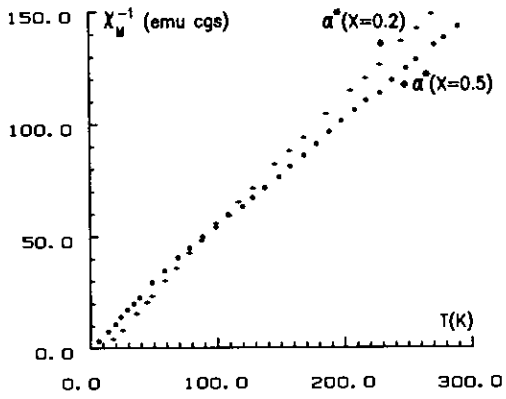

FIG. 4. Thermal variation of reciprocal magnetic susceptibility of the α^* phases for $x = 0.2$ and $x = 0.5$.

TABLE III

EXPERIMENTAL AND THEORETICAL VALUES ($(1 - x)Ni^{2+}$ AND xFe^{3+} IONS ASSUMED WITHIN THE SLAB) OF THE CURIE CONSTANTS AND PARAMAGNETIC CURIE TEMPERATURES OBTAINED FOR THE IRON-SUBSTITUTED α^*-PHASE SERIES ($0.1 \leq x \leq 0.5$)

x	$C_{exp.}$	$C_{theor.}$	θ_p (K)
0	1.18	1.00	10
0.1	1.44	1.34	14
0.2	1.74	1.67	6
0.3	1.84	2.01	−8
0.4	2.10	2.35	−27
0.5	2.11	2.69	−15

The variation with x of the Curie temperature shows clearly that the ferromagnetic interactions are predominant in the unsubstituted phases ($e - p\sigma - p\sigma' - e$ type interaction by correlation). The substitution of iron for nickel leads to the appearance of antiferromagnetic interactions thanks to the strong $t_2 - t_2$ direct overlap. Besides, as a result of the very large interslab distance due to the presence of water molecules and

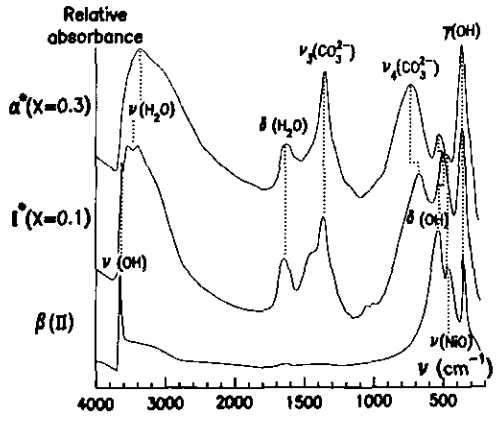

FIG. 5. Infrared spectra of the unsubstituted β(II)-phase and the hydroxides for $x = 0.1$ (interstratified phase I*) and $x = 0.3$ (α*-phase).

inserted anions, no three-dimensional ordering has been detected.

Infrared Spectroscopy

The spectra have been recorded on a Perkin–Elmer 983 spectrometer. In a first step, the measurements have been performed on powders dispersed in Nujol in the 200–4000 cm^{-1} range, but as the main carbonate vibration band was overlapped by a Nujol band, other experiments have been carried out using hexachlorobutadiene in the 1000–4000 cm^{-1} range. The infrared spectra of the nickel hydroxides are given in Fig. 5 for $x = 0.1$ and $x = 0.3$ in comparison with the well known spectrum of the β(II)-phase (*18*). The latter exhibits:

—a narrow band at 3650 cm^{-1} due to the ν(OH) stretching vibration

—bands at 520 cm^{-1} and 350 cm^{-1} corresponding to the hydroxyl group δ(OH) lattice vibration and to the out-of-plane γ(OH) vibration respectively

—the weak Ni–O lattice vibration band around 460 cm^{-1} (*19*).

The substitution of iron for nickel entails strong modifications of the spectrum; one has to notice:

—the appearance of large bands around 3300 cm^{-1} and 1650 cm^{-1} corresponding respectively to the stretching ($\nu(H_2O)$) and bending ($\delta(H_2O)$) modes of water molecules

—the disappearance for $x = 0.3$ of the narrow band at 3650 cm^{-1} that is characteristic of free OH groups (*19*)

—a band at 1360 cm^{-1} which is due to carbonate ions.

For $x = 0.3$, the first two points suggest the presence of water molecules inserted in the interslab space, so that OH groups are hydrogen bonded with water molecules. For $x = 0.1$, the infrared spectrum shows strong similarities with that of the α^* – ($x = 0.3$) phase. Meanwhile the simultaneous presence of the narrow ν(OH) band at 3650 cm^{-1} and the large ones around 3300 cm^{-1} and 1650 cm^{-1} emphasizes the existence of two types of interslab spaces (hydrated α*-type motives and unhydrated β(II)-type motives) that characterize the interstratified structure (I*) (*6*).

The spectra of α*-phases with $x = 0.2$ and $x = 0.4$ have been reported in the 4000–1000 cm^{-1} range in Fig. 6. In both spectra, the band at 1360 cm^{-1} characterizes the ν_3 vibration of carbonate anions in D_{3h} symmetry (*19*). Meanwhile, as previously discussed in the case of the cobalt-substituted α*-phases (*20*), the difference between this value and the ν_3 vibration frequencies of CO_3^{2-} ions in

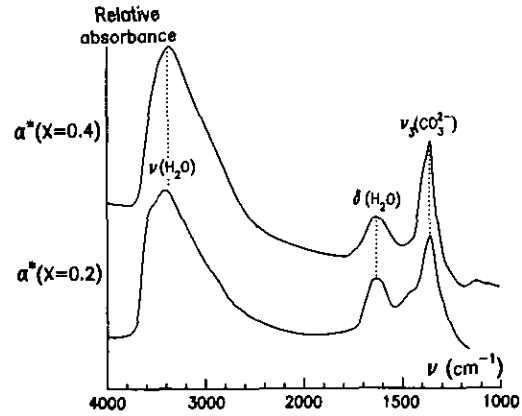

FIG. 6. Infrared spectra of the α*-phases for $x = 0.2$ and $x = 0.4$.

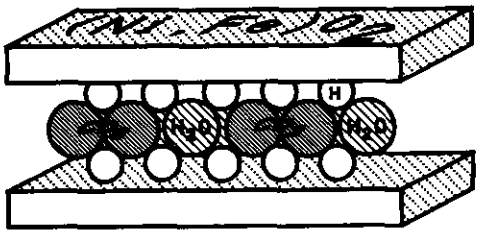

FIG. 7. Schematic representation of the interslab space for an iron-substituted α^*-phase.

$CaCO_3$ (1429 and 1492 cm^{-1}) suggests that the carbonate ions are not in a "free" configuration, but are fully and symmetrically hydrogen bonded with water molecules in the interslab space. A schematic representation of the interslab structure is given in Fig. 7. Moreover, the increase in intensity of the $\nu_3(CO_3^{2-})$ vibration band on the spectra from $x = 0.2$ to $x = 0.4$ evidences an increase in the carbonate concentration with the iron amount. This evolution is fully consistent with the fact that the charge compensation requires, in accordance with the general hydrotalcite formula, a carbonate concentration equal to $x/2$.

From a general point of view, in this family of materials as well as in the Layer Double Hydroxides (LDHs), around 0.50 H_2O molecule per formula unit stays in the intersheet space (*5, 9*). Taking into account that at most one oxygen site per (Ni,Fe) cation is available in the interslab space, at most 0.17 CO_3^{2-} ion can be intercalated. This is corroborated by the chemical analysis performed on the hydroxide series ($0.1 \leq x \leq 0.5$) since the largest carbonate concentration experimentally found is equal to 0.18. As a consequence, for iron concentrations higher than the 0.34 theoretical value the amount of carbonate ions is not sufficient to compensate totally the positive charge excess due to Fe^{3+} ions. The residual charge excess may be neutralized by OH^- ions also inserted in the intersheet space replacing some CO_3^{2-} ions (*6*).

Acknowledgment

The authors thank C. Denage for technical assistance.

References

1. H. BODE, K. DEHMELT, AND J. WITTE, *Electrochim. Acta* **11,** 1079 (1966).
2. C. DELMAS, J. J. BRACONNIER, Y. BORTHOMIEU, AND P. HAGENMULLER, *Mater. Res. Bull.* **22,** 741 (1987).
3. C. DELMAS, Y. BORTHOMIEU, AND C. FAURE, *Proc. Electrochem. Soc. Meeting* **90-4,** 119 (1990).
4. C. FAURE, Y. BORTHOMIEU, C. DELMAS, AND M. FOUASSIER, *J. Power Sources* **36,** 113 (1991).
5. W. T. REICHLE, *Solid State Ionics* **22,** 135 (1986).
6. Y. BORTHOMIEU, Thesis, University of Bordeaux I (1990).
7. A. MENDIBOURE AND R. SCHÖLLHORN, *Rev. Chim. Minér.* **23,** 819 (1986).
8. J. S. WHITE, JR., E. HENDERSON, AND B. MASON, *Am. Mineral.* **52,** 1190 (1967).
9. H. F. W. TAYLOR, *Mineral. Mag.* **39,** 377 (1973).
10. L. DEMOURGUES-GUERLOU, L. FOURNES, AND C. DELMAS, *in* "Proceedings of the Solid State Ionics E-MRS, ICAM 1991" (M. Balkanski, T. Takahashi, and H. L. Tuller, Eds.), Elsevier, Amsterdam (1992).
11. C. DELMAS AND C. FOUASSIER, *Z. Anorg. Allg. Chem.* **420,** 184 (1976).
12. C. DELMAS, C. FOUASSIER, AND P. HAGENMULLER, *B Physica* **99,** 81 (1980).
13. R. D. SHANNON AND C. T. PREWITT, *Acta Crystallogr. Sect. B* **25,** 925 (1969).
14. F. FILLAUX, H. OUBOUMOUR, C. CACHET, J. TOMKINSON, G. J. KEARLEY, AND L. T. YU, *Chem. Phys.* **164,** 311 (1992).
15. L. DEMOURGUES-GUERLOU, L. FOURNES, AND C. DELMAS, submitted for publication.
16. J. J. BRACONNIER, C. DELMAS, C. FOUASSIER, M. FIGLARZ, B. BEAUDOIN, AND P. HAGENMULLER, *Rev. Chim. Miner.* **21,** 496 (1984).
17. C. DELMAS, *in* "Proceeding of the MRS Fall Meeting "Solid State Ionics, Boston," Vol. 210, p. 335 (1990).
18. F. P. KOBER, *J. Electrochem. Soc.* **112,** 1064 (1968).
19. K. NAKAMOTO, "Infrared Spectra of Inorganic and Coordination Compounds," Wiley–Interscience, New York (1963).
20. C. FAURE, C. DELMAS, AND M. FOUASSIER, *J. Power Sources* **35,** 279 (1991).